ICAST2014#Paper ID 009

Enhancement of Aeroelastic Energy Harvesting from Galloping, Vortex-induced Vibrations and Flutter with a Beam Stiffener

Liya Zhao, Jieying Chong, Tian Loong Jonathan NG, Yaowen Yang*

School of Civil and Environmental Engineering, Nanyang Technological University, 50 Nanyang Avenue, Singapore-639798)

Abstract

Wireless sensing systems have been widely exploited in structural health monitoring and environmental monitoring systems in order to ensure the integrity and reliability of infrastructures and their operating environment. Due to the continuously reduced power requirement of wireless sensing nodes, harvesting ambient energy to implement self-powered wireless sensor networks has attracted growing research interests. Aeroelastic energy harvesting focuses on converting aeroelastic energy into electricity by exploring aeroelastic instabilities, such as flutter, vortex-induced vibrations and galloping. A conventional aeroelastic energy harvester consists of a piezoelectric composite cantilever connected with a bluff body at its free end. As an alternative to the conventional aeroelastic energy harvester, in this article, we propose an easy but quite effective method to significantly enhance the power generation capability of aeroelastic energy harvester. The method is to attach a beam stiffener to the substrate of the harvester, which works as an electromechanical coupling magnifier. It is shown to be effective for all the three considered types of harvesters based on galloping, vortex-induced vibration and flutter, leading to a superior performance over the conventional designs without the beam stiffener, with dozens of times increase in power, yet with comparative or even smaller transverse displacement.

1. INTRODUCTION

Implementing self-powered wireless sensor networks (WSNs) by harnessing energy from the ambient environments via various mechanisms has attracted growing research interests [1]. With a target to extract power from ambient wind flows, piezoelectric aeroelastic energy harvesting focuses on converting aeroelastic energy into electricity by exploring aeroelastic instabilities.

A number of studies have been reported in the literature to investigate aeroelastic energy harvesting based on galloping [2-8], vortex-induced vibration [9-11], and flutter [12-15]. A conventional aeroelastic piezoelectric energy harvester (APEH) consists of a piezoelectric composite cantilever connected with a bluff body at its free end. Unlike the target of broadening the working frequency bandwith in the hot area of vibration-based energy harvesting [16-18], the performance enhancement of APEHs aims at reducing the cut-in wind speed, enlarging the effective wind speed range and increasing the harvested power at the

**Corresponding author, cywyang@ntu.edu.sg.

target wind speed. Efforts have been devoted into this through structural modification [19] and circuit optimization [20,21].

We focus on increasing the harvested power level at certain wind speeds via structural modification in this article. We present a convenient method to boost the output power level as well as to enlarge the effective wind speed range. The method is simply to add a beam stiffener to the substrate beside the transducer, as shown in Fig. 1(a). The principle is to amplify the electromechanical coupling by magnifying the slope of the mode shape of the harvester at the edge of the transducer, which is achieved by stiffening the substrate to the right of the transducer (Fig. 1(b)). This is inspired by the fact that the electromechanical coupling is proportional to the difference of mode shape slopes at the starting and ending locations of the transducer [3,6]. Magnified electromechanical coupling results in increased capability of energy conversion thus increased power extracted from the flow. Or from a more intuitive perspective, stiffening the beam section causes redistribution of the strain energy induced by aerodynamic force. The strain energy in the substrate beside the transducer is redistributed to the transducer when it is stiffened, thus boosting the available transferred energy. To investigate the response of the proposed APEH with a beam stiffener and to validate its superior performance over the conventional one, we consider three types of APEHs, which are based on the aeroelasticity principles of galloping (Fig. 1(a)), vortex-induced vibration (VIV) (Fig. 2(a)), and flutter (Fig. 2(b)). Numerical simulations based on the theoretical model demonstrate that by adding a beam stiffener, power generation capabilities of the three types of aeroelastic energy harvesters are significantly increased. While previous research works have focused on a single aeroelasticity phenomenon, the proposed method proposed in this paper give a viable choice to modify the performance of all three types of APEHs for optimal energy harvesting for the WSNs.

2. WORKING PRINCIPLE AND ANALYTICAL MODEL

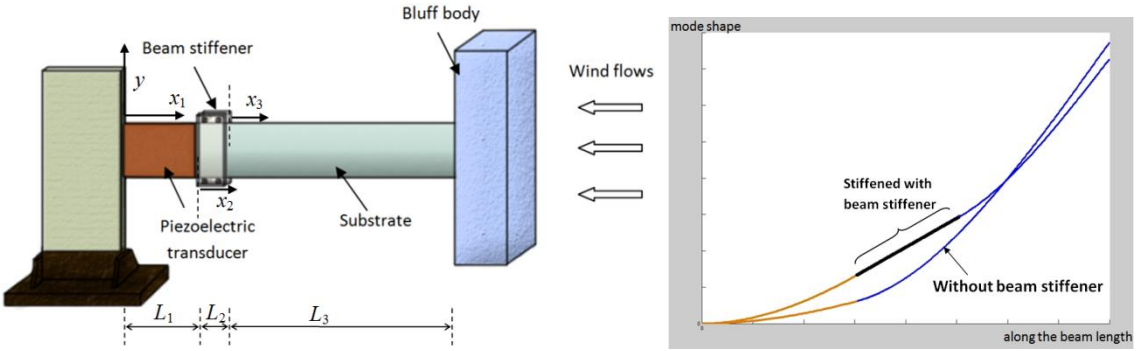

Figure 1. (a) Schematic of the proposed GPEH with a beam stiffener (b) comparison of mode shapes

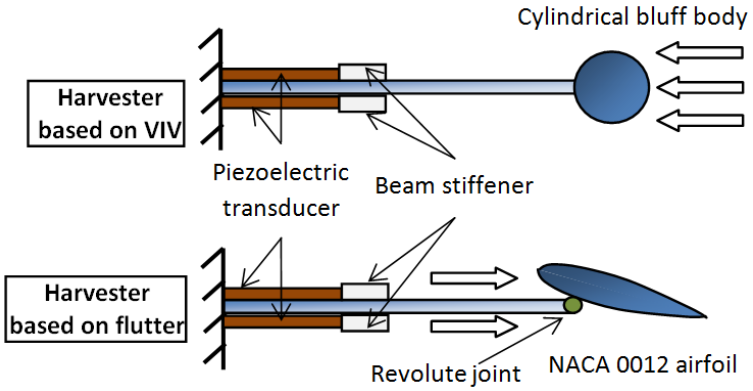

Figure 2. Top view of the modified (a) VIV-based APEH and (b) flutter-based APEH

The galloping-based APEH (GPEH) in Figure 1(a) consists of a cantilever sandwiched by two piezoelectric transducers at the root, and a square-sectioned bluff body fixed at its free end. With the beam stiffener, the whole cantilever is divided into three segments. To study its electro-aero-mechanical responses, we consider a distributed paremeter model based on the Euler-Bernoulli beam theory. Without the aerodynamic force, the equation of motion for undamped free vibration of each segment is

$$EI_i \frac{\partial^4 w_i(x_i,t)}{\partial x_i^4} + m_i \frac{\partial^2 w_i(x_i,t)}{\partial t^2} = 0, \quad i = 1,2,3 \tag{1}$$

where $0<x_1<L_1$, $0<x_2<L_2$, $0<x_3<L_3$; $w_i(x_i, t)$ is the cantilever's transverse deflection; and EI_i and m_i are the bending stiffness and distributed mass of each segment, respectively. To solve the mode shape and natural frequency problems, the boundary conditions at $x_1=0$ and $x_3=L_3$ are determined as

$$w_1(0,t) = 0 \tag{2}$$

$$\frac{\partial w_1(x_1,t)}{\partial t}\Big|_{x_1=0} = 0 \tag{3}$$

$$EI_3 \frac{\partial^2 w_3(x_3,t)}{\partial x_3^2}\Big|_{x_3=L_3} = -J_t \frac{\partial^3 w_3(x_3,t)}{\partial x_3 \partial t^2}\Big|_{x_3=L_3} \tag{4}$$

$$EI_3 \frac{\partial^3 w_3(x_3,t)}{\partial x_3^3}\Big|_{x_3=L_3} = M_t \frac{\partial^2 w_3(x_3,t)}{\partial t^2}\Big|_{x_3=L_3} \tag{5}$$

where M_t and J_t are, respectively, the mass and rotary inertia of the bluff body. The transition conditions at $x_1=L_1$ and $x_2=L_2$ are

$$w_1(L_1,t) = w_2(0,t) \tag{6}$$

$$\frac{\partial w_1(x_1,t)}{\partial x_1}\Big|_{x_1=L_1} = \frac{\partial w_2(x_2,t)}{\partial x_2}\Big|_{x_2=0} \tag{7}$$

$$EI_1 \frac{\partial^2 w_1(x_1,t)}{\partial {x_1}^2}\Big|_{x_1=L_1} = EI_2 \frac{\partial^2 w_2(x_2,t)}{\partial {x_2}^2}\Big|_{x_2=0} \tag{8}$$

$$EI_1 \frac{\partial^3 w_1(x_1,t)}{\partial {x_1}^3}\Big|_{x_1=L_1} = EI_2 \frac{\partial^3 w_2(x_2,t)}{\partial {x_2}^3}\Big|_{x_2=0} \tag{9}$$

$$w_2(L_2,t) = w_3(0,t) \tag{10}$$

$$\frac{\partial w_2(x_1,t)}{\partial x_2}\Big|_{x_2=L_2} = \frac{\partial w_3(x_3,t)}{\partial x_3}\Big|_{x_3=0} \tag{11}$$

$$EI_2 \frac{\partial^2 w_2(x_2,t)}{\partial {x_2}^2}\Big|_{x_2=L_2} = EI_3 \frac{\partial^2 w_3(x_3,t)}{\partial {x_3}^2}\Big|_{x_3=0} \tag{12}$$

$$EI_2 \frac{\partial^3 w_2(x_2,t)}{\partial {x_2}^3}\Big|_{x_2=L_2} = EI_3 \frac{\partial^3 w_3(x_3,t)}{\partial {x_3}^3}\Big|_{x_3=0} \tag{13}$$

$w_i(x_i, t)$ can be expanded with the eigenfunctions $\phi_{ir}(x_i)$ and modal coordinates $\eta_r(t)$ as

$$w_i(x_i,t) = \sum_{r=1}^{\infty} \phi_{ir}(x_i)\eta_r(t), \ i=1,2,3 \tag{14}$$

$\phi_{ir}(x_i)$ are expressed as

$$\phi_{ir}(x_i) = A_{ir}\sin(\beta_{ir}x_i) + B_{ir}\cos(\beta_{ir}x_i) + C_{ir}\sinh(\beta_{ir}x_i) + D_{ir}\cosh(\beta_{ir}x_i), \ i=1,2,3 \tag{15}$$

where

$${\beta_{ir}}^4 = \frac{{\omega_r}^2 m_i}{EI_i} \tag{16}$$

The natural frequencies ω_r and the coefficients A_{ir}, B_{ir}, C_{ir}, and D_{ir} are obtained as a common practice by introducing Equation (14) into (2) to (13) and forcing the resulted 12×12 matrix to be singular. A mass normalization process for $\phi_{ir}(x_i)$ are employed as

$$\sum_{i=1}^{3}\int_0^{L_i} m_i\phi_{ir}(x_i)\phi_{is}(x_i)dx_i + M_t\phi_{3r}(L_3)\phi_{3s}(L_3) + J_t \frac{d\phi_{3r}(x_3)}{dx_3}\Big|_{x_3=L_3}\frac{d\phi_{3s}(x_3)}{dx_3}\Big|_{x_3=L_3} = \delta_{rs} \tag{17}$$

where δ_{rs} is the Kronecker delta. Now, taking into account the electromechanical coupling term and the aerodynamic force, e.g. the galloping force first, substituting Equation (14) into (1), orthogonalizing it with Equation (17) and considering only the fundamental mode yield the modal equation of motion as

$$\ddot{\eta}(t) + 2\zeta\omega_n\dot{\eta}(t) + {\omega_n}^2\eta(t) + \chi V(t) = f_{galloping}(t) \tag{18}$$

where ζ is the modal mechanical damping; ω_n is the fundamental frequency; V is the generated voltage across the external resistive load R; and χ is the modal electromechanical coupling term written as $\chi=\theta[\phi_1'(L_1) - \phi_1'(0)]$ with $\theta=-E_p d_{31} b_p (h_p+h_s)$. E_p, d_{31}, b_p, h_p, and h_s are the Young's modulus, piezoelectric

constant, width and thickness of the piezoelectric transducer and thickness of the substrate, respectively. It is clear that once the geometric and material parameters regarding the piezoelectric cantilever are fixed, θ is constant and χ depends purely on (and is proportional to) the value of $\phi_1'(L_1)$- $\phi_1'(0)$. By varying L_2, $\phi_1'(L_1)$ is altered, influencing electromechanical coupling as well as the total power generation performance. $f_{galloping}$ is the modal galloping force, expressed as

$$f_{galloping}(t) = \phi_3(L_3) \times \frac{1}{2} \rho h l U^2 \sum_{j=1}^{3} A_j \left[\frac{\phi_3(L_3)\dot{\eta}(t)}{U} + \phi_3'(L_3)\eta(t) \right]^j \tag{19}$$

where ρ, h, l, U and A_j are the air density, frontal dimension and length of the bluff body, wind speed, and empirical aerodynamic coefficients, respectively. The electrical circuit equation is obtained via the Kirchhoff laws as

$$\frac{V(t)}{R} + C_p \dot{V}(t) - \chi \dot{\eta}(t) = 0 \tag{20}$$

where C_p is the capacitance of the transducer.

The VIV-based APEH (VIVPEH) (Figure 2(a)) consists of the same pizoelectric cantilever and a cylindrical bluff body fixed at its free end. The circuit equation remains the same while the motion of equation requires the consideration of the fluid-induced damping. The modal equation of motion is

$$\ddot{\eta}(t) + 2\zeta\omega_n\dot{\eta}(t) + \frac{1}{2} C_D \rho h l U \phi_3^2(L_3)\dot{\eta}(t) + \omega_n^2 \eta(t) + \chi V(t) = f_{VIV}(t) \tag{21}$$

$$f_{VIV}(t) = \frac{1}{4}\phi_3(L_3) C_{L0} \rho h l U^2 q(t) \tag{22}$$

where C_D is the mean sectional drag coefficient; C_{L0} is the steady lift coefficient; f_{viv} is the modal VIV force given in Equation (22); and q is obtained from the nonlinear wake oscillator in Equation (23) (Facchinetti et al., 2003), with ε and A being constants obtained from experiments and ω_f being the vortex-shedding frequency. It is common to express ω_f as $\omega_f = 2\pi StU/h$, with St being the Strouhal number.

$$\ddot{q}(t) + \varepsilon\omega_f \left[q^2(t) - 1 \right] \dot{q}(t) + \omega_f^2 q(t) = \frac{A}{h}\phi_3(L_3)\ddot{\eta}(t) \tag{23}$$

Finally, for the flutter-based APEH (FPEH) in Figure 2(b), the motion Equations (24) and (25) are employed. The pizoelectric cantilever is the same with the former two cases, while the bluff body is changed to a NACA0012 airfoil connected to the free end using a revolute joint. The lumped mass M_T, transverse damping C_w, transverse stiffness K_w, and the electromechanical coupling Θ are linked to the distributed parameter model by $M_T = 1/\phi_3^2(L_3)$, $C_w = 2\zeta\omega_n/\phi_3^2(L_3)$, $K_w = \omega_n^2/\phi_3^2(L_3)$ and $\Theta = \chi/\phi_3(L_3)$. I_α, M_w, C_α, K_α and X_G are the rotary moment and the mass of the airfoil (i.e., M_T minus the weight of the revolute joint), damping and rotary stiffness of the revolute joint, and the distance from the airfoil mass center to the revolute joint, respectively. w_t and α are the transverse and rotational displacement of the airfoil, respectively. The flutter lift force and $L_{flutter}$ and moment $M_{flutter}$ are depicted in Equations (26) and (27), which are related to the effective angle of attack $\alpha_{eff} = \alpha + w_t/U + (0.5b - a)\dot{\alpha}/U$. b, S, a, and C_L are the half chord and span of the airfoil, distance from the mid chord to the revolute joint and lift coefficient, respectively. It should be noted that in the circuit equation (20), χ is replaced by Θ for model simulation of flutter-based APEH.

$$M_T \ddot{w}_t(t) + M_w X_G \ddot{\alpha}(t) + C_w \dot{w}_t(t) + K_w w_t(t) + \Theta V(t) = -L_{flutter}(t) \tag{24}$$

$$M_w X_G \ddot{w}_t(t) + I_\alpha \ddot{\alpha}(t) + C_\alpha \dot{\alpha}(t) + K_\alpha \alpha(t) = M_{flutter}(t) \tag{25}$$

$$L_{flutter}(t) = \rho b S U^2 C_L \left[\alpha_{eff}(t) - c_3 \alpha_{eff}{}^3(t) \right] \tag{26}$$

$$M_{flutter}(t) = \left(\frac{b}{2} + a \right) L_{flutter}(t) \tag{27}$$

3. PARAMETRIC STUDY AND DISCUSSION

3.1 Variation of the fundamental mode shape and fundamental frequency of the cantilever with L_2

The parameters of the harvester are taken as: Young's modulus of the substrate E_s=69GPa and the transducer E_p=23.3GPa, d_{31}=-174pm/V, b_p=b_s=34mm, h_p=0.5mm, h_s=0.6mm, thickness of acrylic h_{bs}=45mm, mass density of the substrate, transducer and acrylic are, respectively, m_s=2700kg/m^3, m_p=3825kg/m^3 and m_{bs}=1180kg/m^3, L_1=61mm, and L_2+L_3=209mm. During the test, three values of L_2, 20mm, 50mm, and 80mm are considered, i.e., three beam stiffeners with different length are tested. The average power is calculated with $P=V_{RMS}^2/R$ where the RMS voltage $V_{RMS}=V/\sqrt{2}$.

With the aforementioned theoretical models, numerical calculations of responses of power P, displacement of the bluff body w_t and efficiency η^* are conducted for L_2=20, 50, 80, 110, 140 and 209mm. Before proceeding to these results, we should take a further look at the variation of $\phi(x)$ and ω_n (Fig. 3), both of which have great effects on the responses. With L_2 increases from 0 to 140mm, $\phi_1'(L_1)$ gradually increases, leading to increasing electromechanical coupling. Yet when L_2 further increases to 209mm, $\phi_1'(L_1)$ decreases. This is because that the added mass by the stiffener (acrylic material) becomes prevalent and induces greatly increased effective mass M_{eff}, which is associated with the obviously decreased $\phi_3(L_3)$. Similarly, ω_n gradually increases due to the extra stiffness induced by L_2 until 110mm, then decreases when L_2 further increases due to the increased M_{eff}.

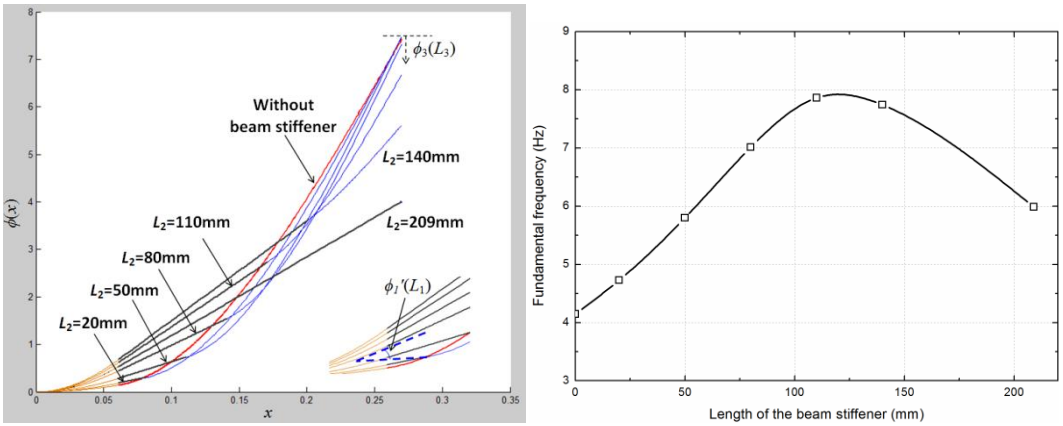

Figure 3. (a) Variation of fundamental mode shapes and (b) fundamental frequencies with the length of beam stiffener

3.2 Effects of the wind speed and length of beam stiffener on the harvester's response

In the following theoretical simulations for the GPEH, VIVPEH and FPEH, parameters regarding the piezoelectric cantilevers and masses of the bluff bodies (for the flutter, it is the sum of the masses of the airfoil and revolute joint) are identical, such that the $\phi(x)$ and ω_n for all harvesters are the same as those shown in Fig. 3. The variations of P and w_t at optimal load R_{opt} (which gives the maximum P over the whole R range) with U for the three types of APEHs are plotted in Fig. 4. Figure 4(a) clearly indicates the dramatic enhancement of power output for the GPEH with the beam stiffener, especially for larger values of L_2 at high U. The growing rate of P (i.e. the slope of the curve of P versus U) increases with L_2. At a small wind speed U=3m/s, the conventional GPEH generates a power of P= 0.60mW, while the GPEH with a stiffener of L_2=80mm generates P=1.49mW; at U=5m/s, P from the conventional GPEH is 1.42mW, while it is increased to 7.57mW with a beam stiffener of L_2=110mm; at a large U=15m/s, the conventional GPEH provides P=3.10mW, while the stiffened GPEH with L_2=209mm achieves P=139.74mW. These correspond to 1.5, 4.3 and 44.0 times increase of power output at the respective wind speed. The dashed curve depicts the envelope of achievable power by the GPEH with beam stiffener. Nevertheless, the U_{cr} of GPEH with beam stiffener also increases with L_2. This drawback can be overcome by a pre-measurement of the wind speed at the target location of harvesters or WSNs, employing the optimal L_2 to achieve the best power generating performance according to Fig. 4(a). The variation of w_t with U is presented in Fig. 4(b), which clearly shows that the stiffened GPEHs have smaller displacement compared to the conventional counterparts, except for L_2=209mm. This further confirms the benefit of the beam stiffener of fatigue mitigation and durability enhancement.

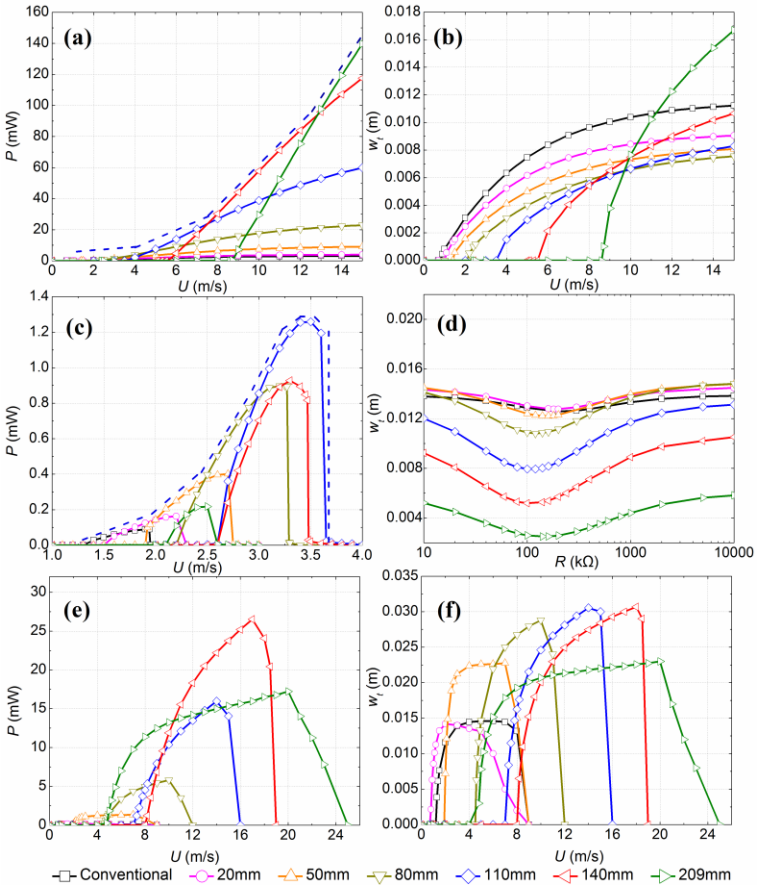

Fig. 4. Responses of (a) (b) GPEH (c) (d) VIVPEH and (e) (f) FPEH. (a) (c) (e) P versus U, (b) (f) w_t versus U and (d) w_t versus R. Dashed curves represents the envelope of attainable P.

For the VIVPEH, high amplitude oscillations occur in a lock-in region where the vortex shedding frequency gets close to the structure's natural frequency. As shown in Fig. 4(c) (with the parameters C_D=2.0, C_{L0}=0.3, ε=0.3, A=12 [22], and St=0.105 [10]), there exist the cut-in and cut-out wind speeds for the VIVPEH. As expected, the lock-in region shifts to higher U with increasing L_2 until 110mm, then shifts to smaller U when L_2 further increases. This agrees to the variation of ω_n in Fig. 3(b). The maximum P of 0.09mW is achieved by the conventional VIVPEH at U=1.94m/s, while the maximum P of 1.26mW is obtained by the stiffened VIVPEH at U=3.50m/s with L_2=110mm, corresponding to 13.1 times increase. Besides the enhancement of power, the beam stiffener brings an broadened lock-in region as well, i.e., from 1.20m/s to 1.96m/s for the conventional VIVPEH, and from 2.50m/s to 3.62m/s for the stiffened one with L_2=110mm. The dashed curve gives the attainable power envelope of the stiffened VIVPEH, which can be achieved by appropriately adjusting L_2 according to the pre-tested target U. Figure 4(d) clearly indicates that enhanced power is reached with comparable or even smaller displacement. For the FPEH with the considered parameters (I_α=24.3g·cm^2, M_w=7.84g, C_α=1.63e-5N·m·s, K_α=0.0019N·m/rad, X_G=3mm, b=42mm, S=52mm, a=-21mm, C_L=6.283, and c_3=6.5), subcritical Hopf bifurcation is observed. Moreover, there exist cut-out wind speeds when U grows to the higher range. Enhanced power output is also achieved (Fig. 4(e)), e.g., at U=5m/s, P is increased from 0.096mW for the conventional FPEH to 1.28mW, i.e., 12.3 times increase for the stiffened one with L_2=50mm. More obvious enhancement is observed at high U range, e.g., at U=17m/s, P=26.52mW is obtained with L_2=140mm. Inspecting the responses of w_t shown in Fig. 4(f), it is seen that the involvement of the beam stiffener induces almost doubled displacement for FPEH. The maximum w_t is around 30mm, still acceptable for the 270mm cantilever, but the fatigue problem requires attention when employing the stiffened FPEH.

5. CONCLUSION

This article theoretically demonstrates that with the easy method of adding a beam stiffener, power generation capabilities of the galloping-based, VIV-based and flutter-based aeroelastic energy harvesters are significantly increased. The maximum power can be boosted by more than a dozen times, with comparative or even smaller displacement, thus without aggravating the fatigue problem. For the VIV-based harvester, the lock-in region is also broadened. The flutter-based harvester is found to have the highest efficiency, and is able to operate in large range of wind speeds; the VIV-based harvester is recommended for environments with unchanged and small wind speed, while galloping-based harvester has much higher power output than the former two at high wind speed thus is suggested for scenarios with sufficiently strong wind flows.

REFERENCES

1. Anton S R and Sodano H A 2007 A review of power harvesting using piezoelectric materials (2003–2006) *Smart materials and Structures* 16: R1.
2. Barrero-Gil A, Alonso G and Sanz-Andres A 2010 Energy harvesting from transverse galloping *Journal of Sound and Vibration* 329: 2873-2883.

3. Abdelkefi A, Yan Z and Hajj M R 2013 Modeling and nonlinear analysis of piezoelectric energy harvesting from transverse galloping *Smart materials and Structures* 22: 025016.
4. Sirohi J and Mahadik R 2011 Piezoelectric wind energy harvester for low-power sensors *Journal of Intelligent Material Systems and Structures* 22: 2215-2228.
5. Yang Y, Zhao L and Tang L 2013 Comparative study of tip cross-sections for efficient galloping energy harvesting *Applied Physics Letters* 102: 064105.
6. Zhao L, Tang L and Yang Y 2013 Comparison of modeling methods and parametric study for a piezoelectric wind energy harvester *Smart materials and Structures* 22: 125003.
7. Tang L, Zhao L, Yang Y and Lefeuvre E 2014 Equivalent Circuit Representation and Analysis of Galloping-Based Wind Energy Harvesting *IEEE/ASME Transactions on Mechatronics*: DOI:10.1109/TMECH.2014.2308182.
8. Bibo A and Daqaq M 2014 On the optimal performance and universal design curves of galloping energy harvesters *Applied Physics Letters* 104: 023901.
9. Pobering S, Ebermeyer S and Schwesinger N 2009 Generation of electrical energy using short piezoelectric cantilevers in flowing media *SPIE Smart Structures and Materials+ Nondestructive Evaluation and Health Monitoring.* International Society for Optics and Photonics, 728807-728807-728808.
10. Akaydin HD, Elvin N and Andreopoulos Y 2012 The performance of a self-excited fluidic energy harvester *Smart materials and Structures* 21: 025007.
11. Dai H, Abdelkefi A and Wang L 2014 Theoretical modeling and nonlinear analysis of piezoelectric energy harvesting from vortex-induced vibrations *Journal of Intelligent Material Systems and Structures*: DOI: 10.1177/1045389X14538329.
12. De Marqui C and Erturk A 2013 Electroaeroelastic analysis of airfoilbased wind energy harvesting using piezoelectric transduction and electromagnetic induction *Journal of Intelligent Material Systems and Structures* 24: 846-854.
13. Bryant M and Garcia E. (2011) Modeling and testing of a novel aeroelastic flutter energy harvester. *Journal of Vibration and Acoustics* 133: 011010.
14. Erturk A, Vieira W, De Marqui Jr C and Inman D J 2010 On the energy harvesting potential of piezoaeroelastic systems *Applied Physics Letters* 96: 184103.
15. Bibo A and Daqaq M 2013 Investigation of concurrent energy harvesting from ambient vibrations and wind using a single piezoelectric generator *Applied Physics Letters* 102: 243904.
16. Aladwani A, Arafa M, Aldraihem O and Baz A 2012 Cantilevered piezoelectric energy harvester with a dynamic magnifier *Journal of Vibration and Acoustics* 134: 031004.
17. Zhou S, Cao J, Inman D J, Lin J, Liu S and Wang Z 2014 Broadband tristable energy harvester: Modeling and experiment verification *Applied Energy* 133: 33-39.
18. Tang L and Yang Y 2012 A nonlinear piezoelectric energy harvester with magnetic oscillator *Applied Physics Letters* 101: 094102.
19. Zhao L, Tang L and Yang Y 2014 Enhanced piezoelectric galloping energy harvesting using 2 degree-of-freedom cut-out cantilever with magnetic interaction *Japanese Journal of Applied Physics* 53: 060302.
20. Bryant M, Schlichting A D and Garcia E 2013 Toward efficient aeroelastic energy harvesting: device performance comparisons and improvements through synchronized switching *SPIE Smart Structures and Materials+ Nondestructive Evaluation and Health Monitoring.* International Society for Optics and Photonics, 868807-868807-868810.
21. Zhao L, Tang L, Wu H and Yang Y 2014 Synchronized charge extraction for aeroelastic energy harvesting *SPIE Smart Structures and Materials+ Nondestructive Evaluation and Health Monitoring.* International Society for Optics and Photonics, 90570N-90570N-90513.
22. Facchinetti M L, de Langre E and Biolley F 2004 Coupling of structure and wake oscillators in vortex-induced vibrations *Journal of Fluids and structures* 19: 123-140.